Electronic Supplementary Material (ESI) for Journal of Materials Chemistry A.

Supporting Information for

Highly stable supercapacitors with MOF-derived Co_9S_8/carbon electrodes for high rate electrochemical energy storage

Shuo Zhang [a], Daohao Li [a], Shuai Chen [b], Xianfeng Yang [c], Xiaoliang Zhao [a], Quansheng Zhao*[,a], Sridhar Komarneni [d] and Dongjiang Yang*[,a,e,f]

[a]Collaborative Innovation Centre for Marine Biomass Fibres, Materials and Textiles of Shandong Province; College of Chemical and Environmental Engineering, Qingdao University, Qingdao, P R China.

[b]State Key Laboratory of Coal Conversion Institute of Coal Chemistry Chinese Academy of Science Taiyuan 030001, China.

[c]Analytical and Testing Centre South China University of Technology Guangzhou 510640, China.

[d]Department of Ecosystem Science and Management and Materials Research Institute, Materials Research Laboratory, The Pennsylvania State University, University Park, PA 16802, USA.

[e]Queensland Micro- and Nanotechnology Centre (QMNC), Griffith University, Nathan, Brisbane, Queensland 4111, Australia.

[f]Key Laboratory of Coal Science and Technology, Taiyuan University of Technology, Ministry of Education and Shanxi Province, Taiyuan 030024, P. R. China.

*To whom correspondence should be addressed. E-mail: zqs0811@sina.com; d.yang@qdu.edu.cn.

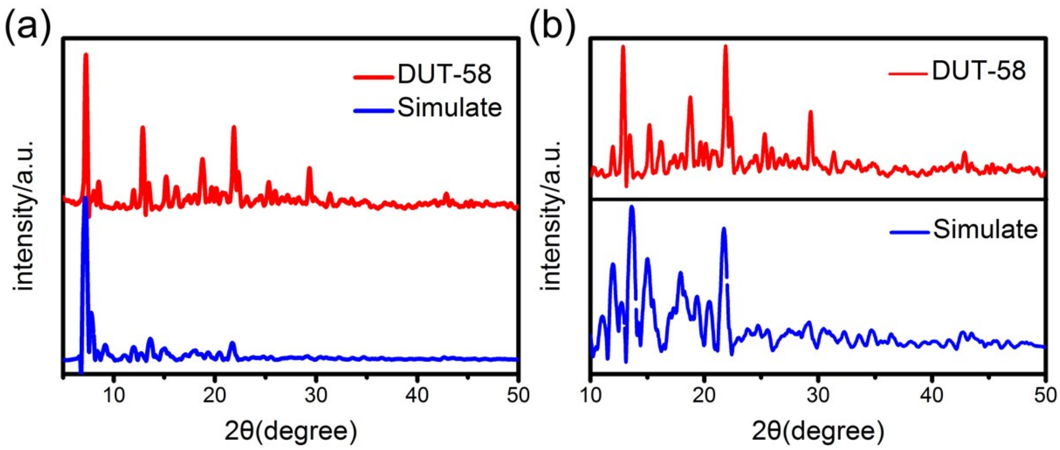

Fig. S1. Experimental and simulated XRD patterns of DUT-58 (a) in the range of 5 ~ 50° and (b) in the range of 10 ~ 50° with amplified simulated data.

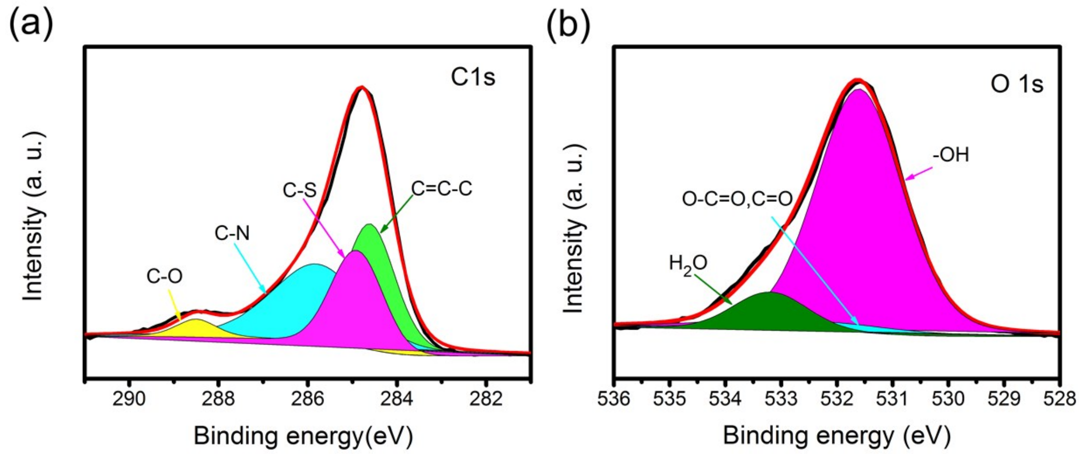

Fig. S2 XPS spectra of (a) C 1s and (b) O 1s for Co_9S_8/NS-C-1.5 h.

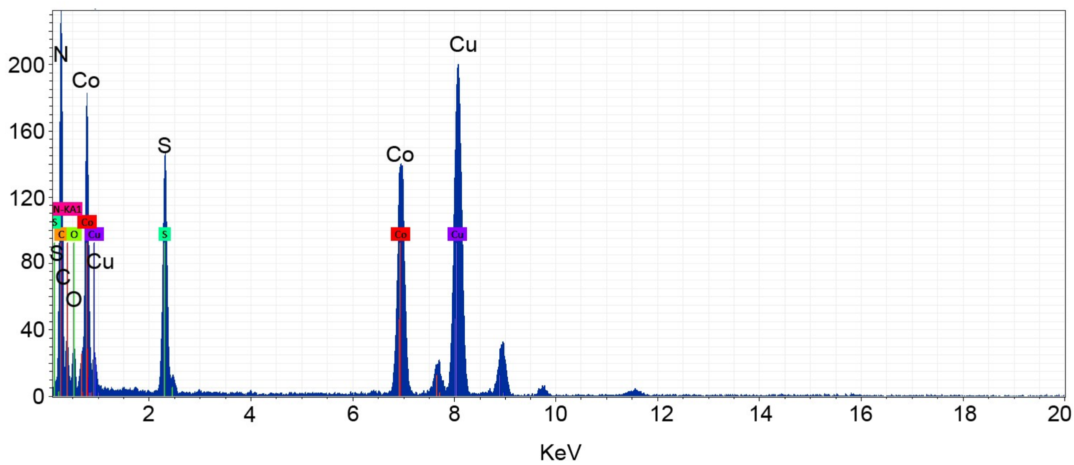

Fig. S3 EDX pattern of the as-prepared Co_9S_8/NS-C-1.5 h.

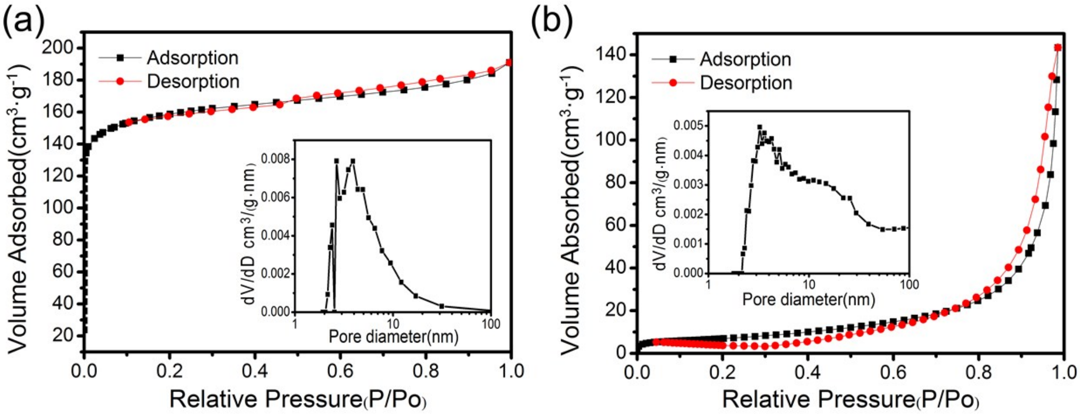

Fig. S4 N_2 sorption isotherms of DUT-58 (a) before and (b) after the confinement treatment. The insets are the corresponding pore size distributions for DUT-58 (a) before and (b) after the confinement of TAA.

The decomposition formula of TAA during the thermal pyrolysis is:

$$CH_3CSNH_2 + 4H_2O \rightarrow H_2S + NH_3 + CO_2 + 4H_2 \qquad (1)$$

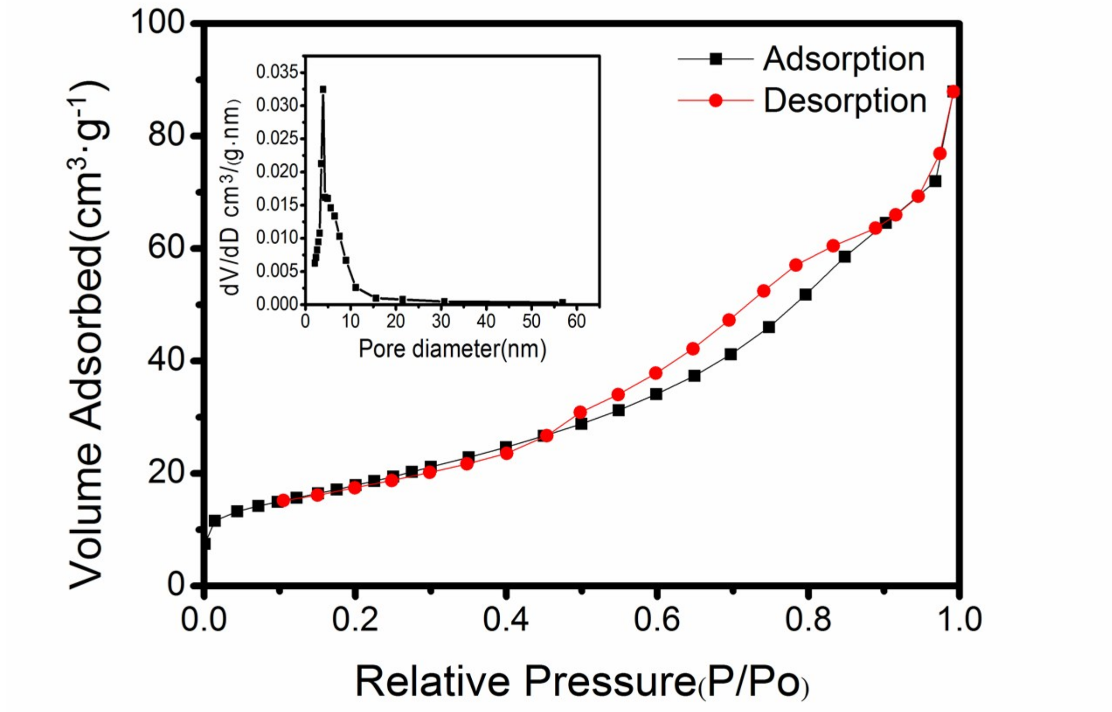

Fig. S5 N_2 sorption isotherms of Co_9S_8/NS-C-1.5 h composite. The inset shows the corresponding pore size distribution.

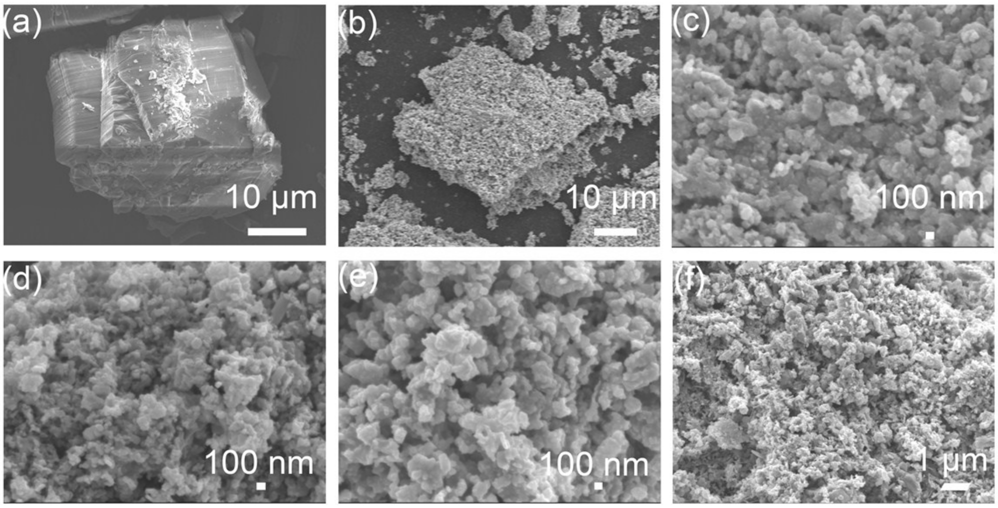

Fig. S6 SEM images of DUT-58 and Co_9S_8/NS-C-t. (a) DUT-58, (b, c) Co_9S_8/NS-C-1.5 h, (d) Co_9S_8/NS-C-0 h, (e) Co_9S_8/NS-C-1 h and (f) Co_9S_8/NS-C-2 h.

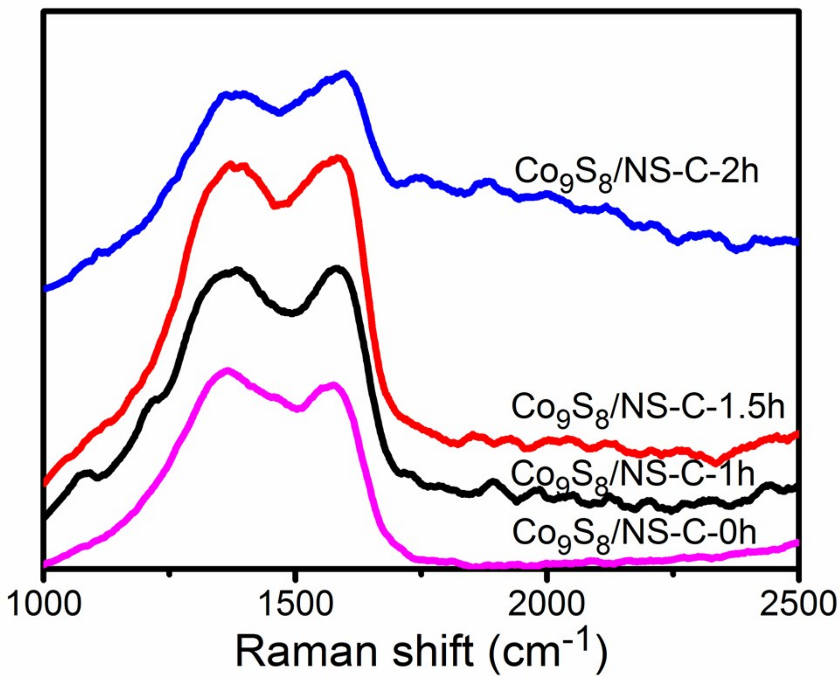

Fig. S7 Raman spectra of Co_9S_8/NS-C-t composites.

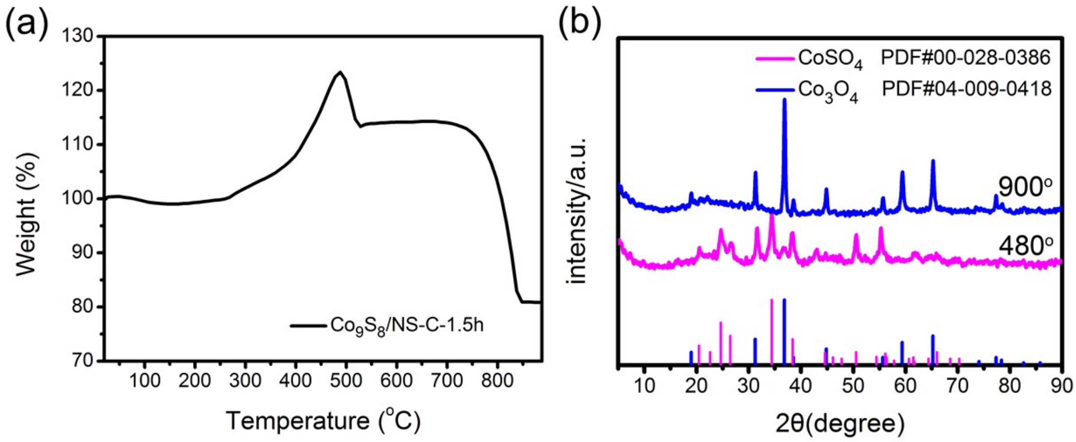

Fig. S8 TG and the corresponding XRD patterns of Co_9S_8/NS-C-1.5 h.

To evaluate the amount of carbon in Co_9S_8/NS-C-1.5 h material, the thermogravimetric (TG) analysis for Co_9S_8/NS-C-1.5 h was carried out in air from 25 to 900 °C, and the corresponding TG curve is shown in Fig. S8. The sample Co_9S_8/NS-C-1.5 h is very stable at temperatures below 200 °C. With increasing temperature, an obvious weight increase takes place from 268 °C to ~ 487 °C. This weight increase is mainly attributed to the partial oxidation of Co_9S_8 NPs to form $CoSO_4$. Above 487 °C, the weight reduction is mainly due to the oxidation of $CoSO_4$ to Co_3O_4 and the removal of amorphous carbon from the composites. At higher than 670 °C, graphitic carbon of the composite gradually disappeared. When the testing temperature is higher than 858 °C, the weight becomes constant and the product is confirmed to be Co_3O_4. During the whole measurement range, the total weight loss is about 19.16%. From this final weight loss value, we estimated that the amount of carbon in Co_9S_8/NS-C-1.5 h is about 12 wt %.

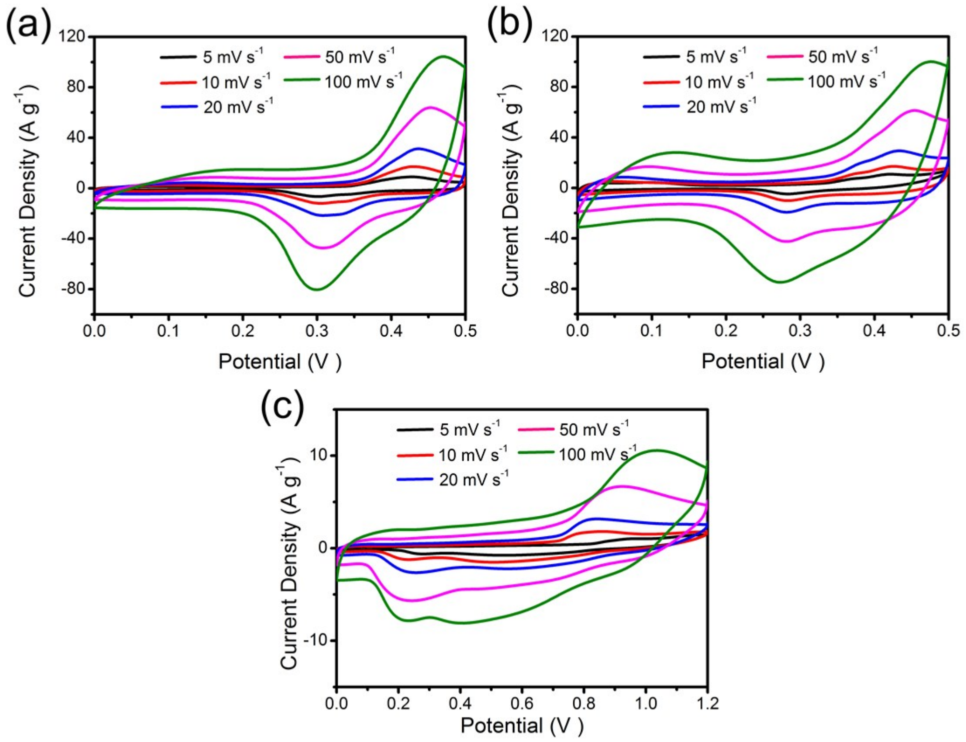

Fig. S9 CV curves of the Co_9S_8/NS-C composite electrodes. (a) Co_9S_8/NS-C-0 h, (b) Co_9S_8/NS-C-1 h and (c) Co_9S_8/NS-C-2 h at scan rates 5, 10, 20, 50 and 100 mV s^{-1}.

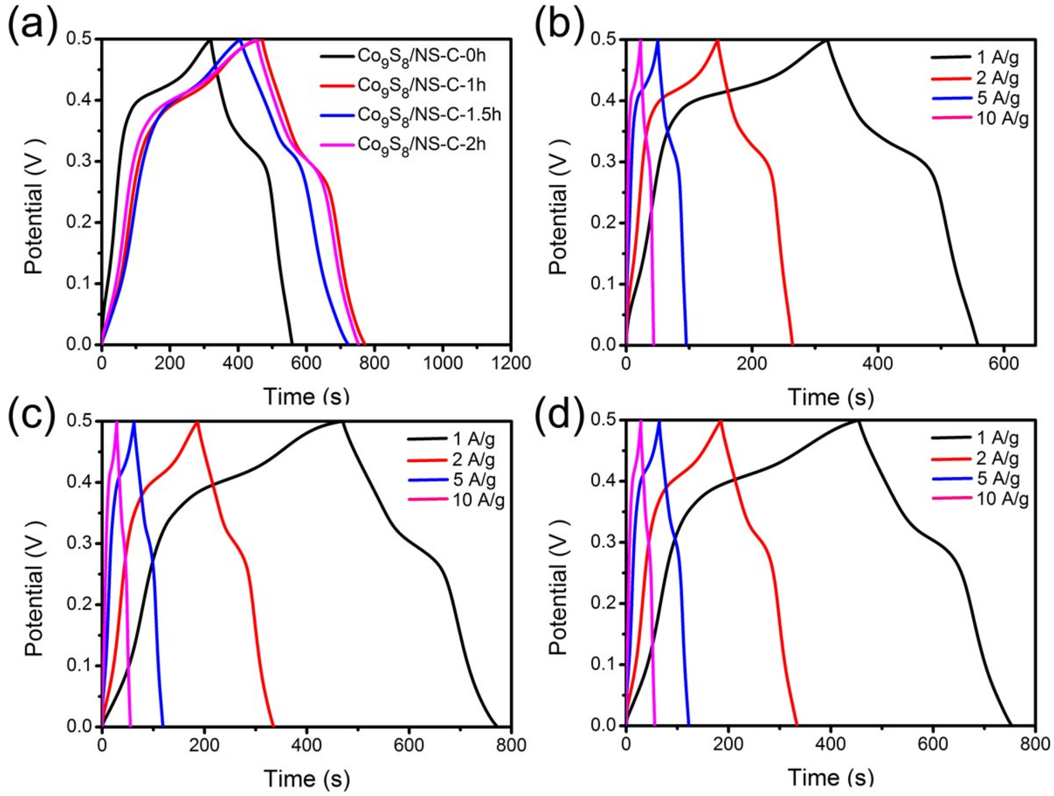

Fig. S10 Galvanostatic charge/discharge curves of the Co_9S_8/NS-C electrodes. (a) Co_9S_8/NS-C-t at 1 A g^{-1}. (b) Co_9S_8/NS-C-0 h, (c) Co_9S_8/NS-C-1 h and (d) Co_9S_8/NS-C-2 h at different current densities.

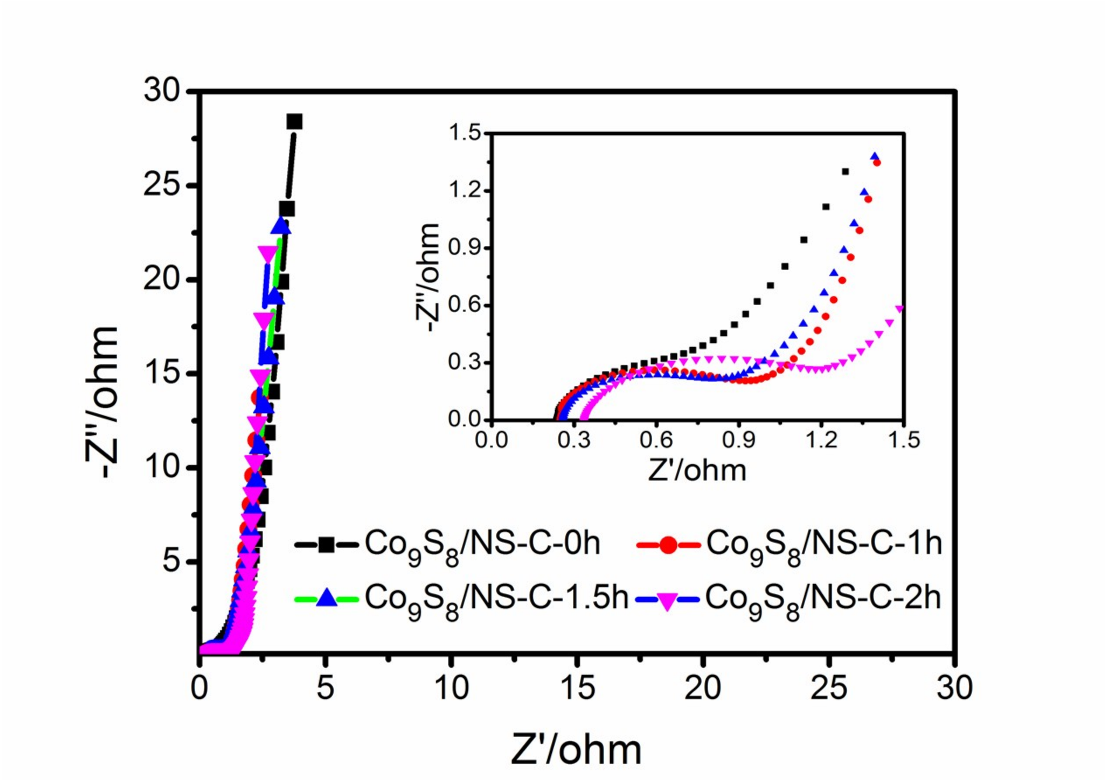

Fig. S11 EIS Nyquist plots of Co_9S_8/NS-C-t electrodes. Inset: EIS Nyquist plots with zoomed data at the high frequency region.

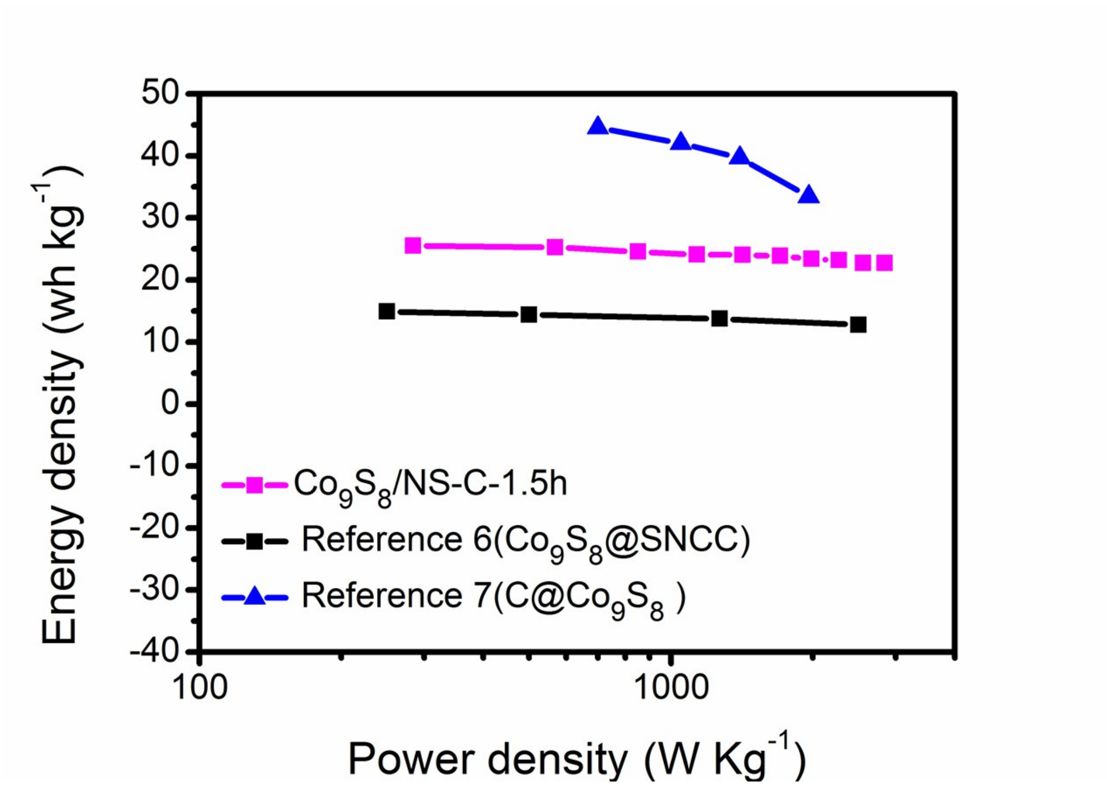

Fig. S12 Ragone plots of Co_9S_8/NS-C-1.5 h and other related electrodes.

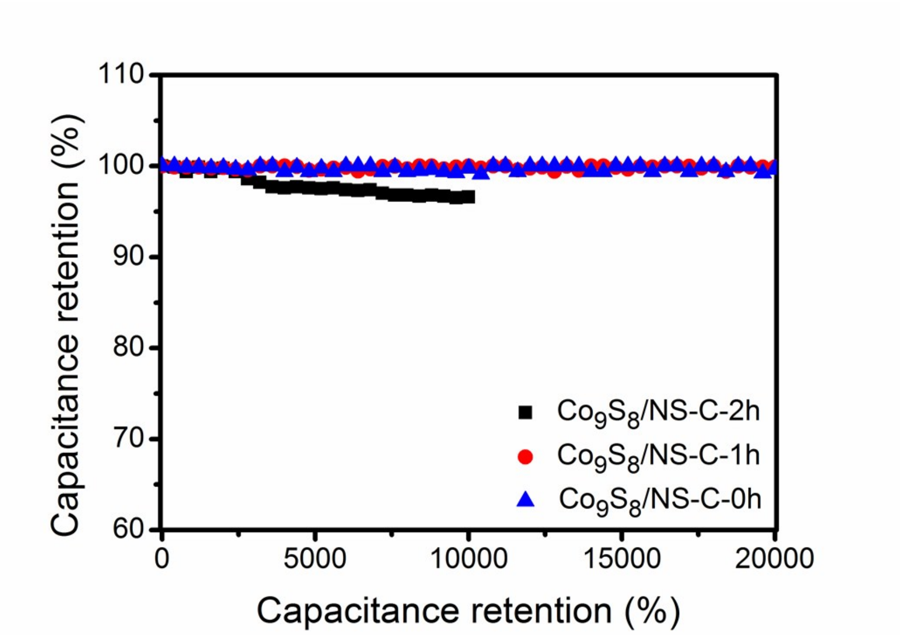

Fig. S13 The cycling performance at the current density of 10 A g^{-1} of Co_9S_8/NS-C-t electrodes.

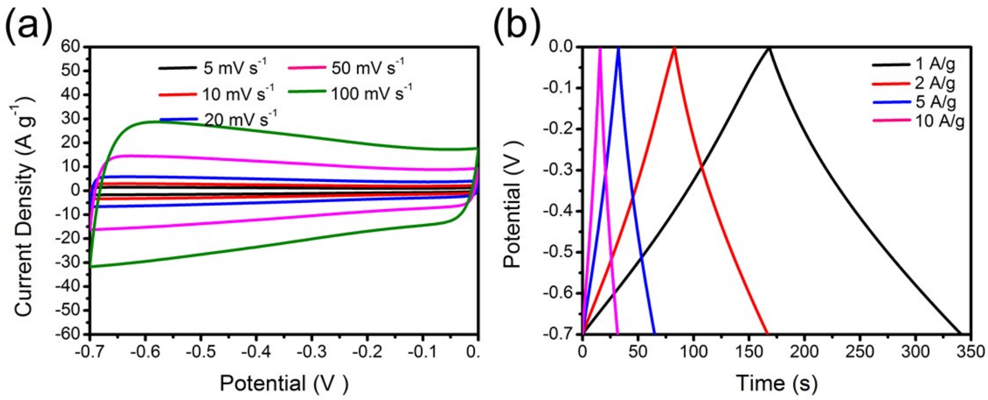

Fig. S14 (a) CV curves and (b) Galvanostatic charge/discharge curves of the AC electrode.

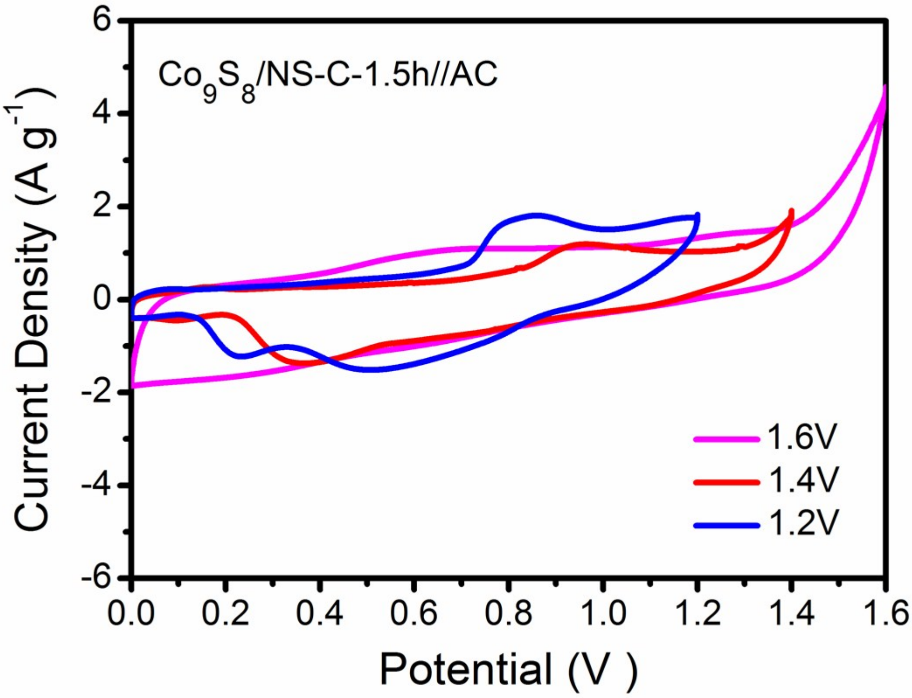

Fig. S15 Cyclic voltammograms of optimized Co_9S_8/NS-C-1.5h//AC asymmetric hybrid supercapacitor at different potential windows at a scan rate of 10 mV s^{-1}.

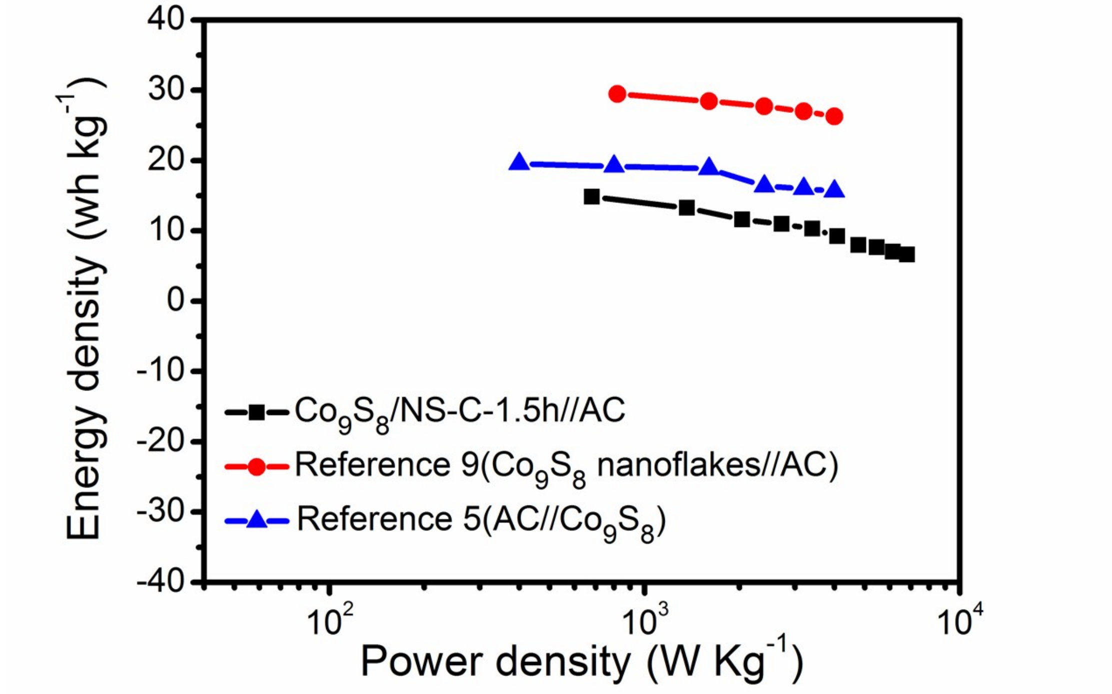

Fig. S16 Ragone plots of Co_9S_8/NS-C-1.5h//AC and other related asymmetric hybrid supercapacitors.

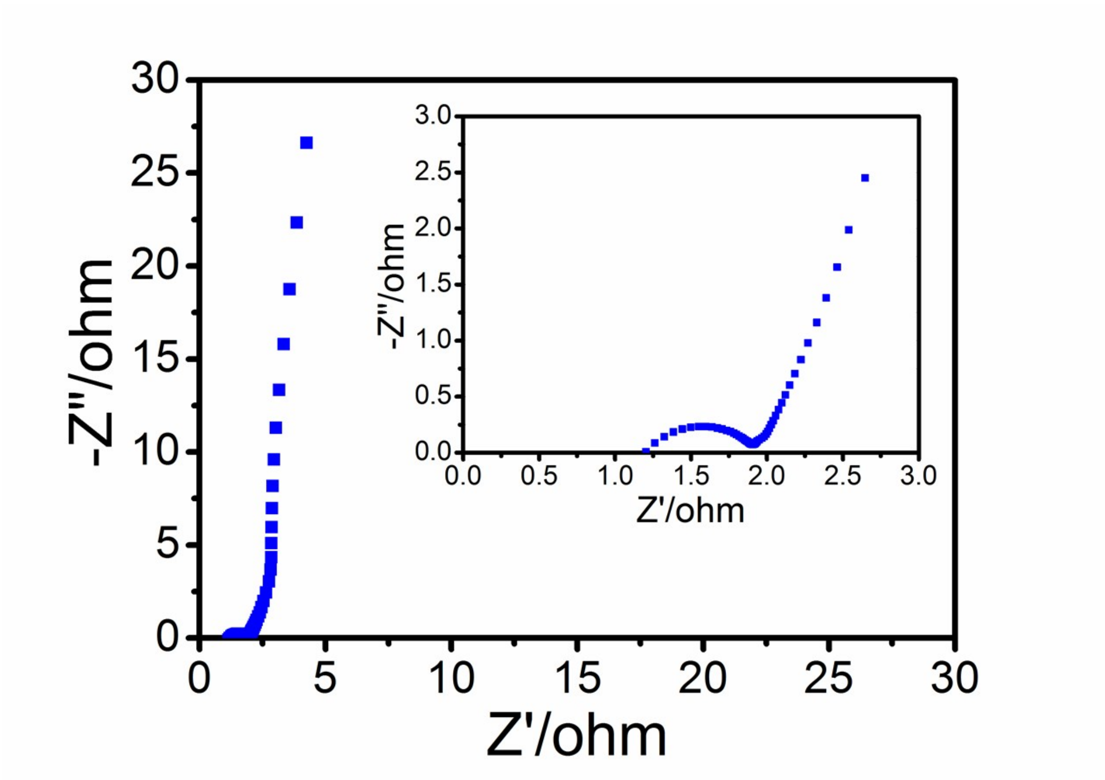

Fig. S17 EIS Nyquist plot of Co_9S_8/NS-C-1.5h//AC asymmetric hybrid supercapacitor. (The inset shows EIS Nyquist plot with zoomed data at the high frequency region).

Table S1 Comparison of various Co_9S_8-based electrodes and asymmetric hybrid supercapacitor (AHS) in recent years as supercapacitors.

Electrode	Electrolyte	Stability	Specific capacitances	Rate capability	Refs
Co_9S_8/NS-C	6.0 M KOH	**140000** cycles **99.8%**	734.09 F g^{-1}@1 A g^{-1} 653.64 F g^{-1}@10 A g^{-1}	89 %	This work
Co_9S_8/NS-C-1.5h//AC		**2000** cycles 99.5%	75.6 F g^{-1}@1 A g^{-1} 32.41 F g^{-1}@10 A g^{-1} (AHS)	42.87%	
Co_9S_8@ $Ni(OH)_2$	2.0 M KOH	**2000** cycles **100%**	1620 F g^{-1}@0.5 A g^{-1} 1227 F g^{-1}@20 A g^{-1}	75.78 %	1
Co_9S_8/NF	2.0 M KOH	**2000** cycles **94.4%**	1645 F g^{-1}@3 A g^{-1} 1309 F g^{-1}@45 A g^{-1}	80 %	2
Co_9S_8	3.0 M KOH	**2000** cycles **91.4%**	1775 F g^{-1}@4 A g^{-1} 1483 F g^{-1}@24 A g^{-1}	83.5 %	3
Co_9S_8	6.0 M KOH	**60** cycles **100%**	306.1 F g^{-1}@0.1 A g^{-1} 224 F g^{-1}@1 A g^{-1}	73.2 %	4
Co_9S_8	2.0 M KOH	**1500** cycles **100%**	520 F g^{-1}@0.5 A g^{-1} 291.2 F g^{-1}@8 A g^{-1}	56 %	5
AC//Co_9S_8		**2000** cycles 100%	55 F g^{-1}@0.5 A g^{-1} 44 F g^{-1}@5 A g^{-1} (AHS)	**80 %**	
Co_9S_8@S,N-doped carbon cuboid	6.0 M KOH	**2000** cycles **98%**	429 F g^{-1}@1 A g^{-1} 336 F g^{-1}@50 A g^{-1}	78.32 %	6
C@Co_9S_8	2.0 M KOH	**3000** cycles **88.5%**	654 F g^{-1}@2 A g^{-1} 491 F g^{-1}@8 A g^{-1}	75.08 %	7
Co_9S_8	6.0 M KOH	**1000** cycles **90.4%**	273.7 F g^{-1}@1 A g^{-1}		8
Co_9S_8 nanoflakes//AC	30% KOH	**5000** cycles **90%**	82.9 F g^{-1}@1.25 A g^{-1} 73.92F g^{-1}@5 A g^{-1} (AHS)	89%	9

References

1 J. Wen, S. Z. Li, B. Li, Z. C. Song, H. N. Wang, R. Xiong and G. J. Fang, *J. Power Sources,* 2015, **284**, 279-286.

2 H. Li, Y. H. Gao, Y. D. Shao, Y. T. Su and X. W. Wang, *Nano lett.*, 2015, **15**, 6689-6695.

3 J. Pu, Z. H. Wang, K. L. Wu, N. Yu and E. H. Sheng, *Phys.Chem.Chem.Phys.*, 2014, **16**, 785-791.

4 L. P. Zhang, Y. R. Wang, W. Zhou, G. S. Song and S. Q. Cheng, *Int. J. Electrochem. Sci.*, 2016, **11**, 1541-1548.

5 B. Li, Y. X. Hu, J. J. Li, M. C. Liu, L. B. Kong, Y. M. Hu and L. Kang, *Metals*, 2016, **6**, 142.

6 S. W. Liu, M. Y. Tong, G. Q. Liu, X. Zhang, Z. M. Wang, G. Z. Wang, W. P. Cai, H. M. Zhang and H. J. Zhao, *Inorg. Chem. Front.*, 2017, **4**, 491-498.

7 T.Wu, X. L. Ma, T. Zhu, *Mater. Lett.*, 2016, **183**, 290-295.

8 L. Yin, L. Q. Wang, X. H. Liu, Y. S. Gai, L. H. Su, B. H. Qu and L. Y. Gong, *Eur. J. Inorg. Chem.*, 2015, **2015**, 2457-2462.

9 R. B. Rakhi, N. A. Alhebshi. D. H. Anjum and H. N. Alshareef, *J. Mater. Chem. A*., 2014, **2**, 16190-16198.